



HAL
open science

Carbazole-fused coumarin based oxime esters (OXEs): efficient photoinitiators for sunlight driven free radical photopolymerization

Yijun Zhang, Zheng Liu, Timur Borjigin, Bernadette Graff, Fabrice Morlet-Savary, Michael Schmitt, Didier Gigmes, Frédéric Dumur, Jacques Lalevée

► To cite this version:

Yijun Zhang, Zheng Liu, Timur Borjigin, Bernadette Graff, Fabrice Morlet-Savary, et al.. Carbazole-fused coumarin based oxime esters (OXEs): efficient photoinitiators for sunlight driven free radical photopolymerization. *Green Chemistry*, 2023, 25 (17), pp.6881-6891. 10.1039/D3GC02004E . hal-04221164

HAL Id: hal-04221164

<https://hal.science/hal-04221164v1>

Submitted on 28 Sep 2023

HAL is a multi-disciplinary open access archive for the deposit and dissemination of scientific research documents, whether they are published or not. The documents may come from teaching and research institutions in France or abroad, or from public or private research centers.

L'archive ouverte pluridisciplinaire **HAL**, est destinée au dépôt et à la diffusion de documents scientifiques de niveau recherche, publiés ou non, émanant des établissements d'enseignement et de recherche français ou étrangers, des laboratoires publics ou privés.

Carbazole-fused coumarin based oxime esters (OXEs): efficient

photoinitiators for sunlight driven free radical photopolymerization

Yijun Zhang,^{†,‡} Zheng Liu,[§] Timur Borjigin,^{†,‡} Bernadette Graff,^{†,‡} Fabrice Morlet-Savary,^{†,‡} Michael Schmitt,^{†,‡} Didier Gimes,[§] Frédéric Dumur,^{§,*} Jacques Lalevée^{†,‡,*}

[†] Université de Haute-Alsace, CNRS, IS2M UMR 7361, F-68100 Mulhouse, France

[‡] Université de Strasbourg, France

[§] Aix Marseille Univ, CNRS, ICR, UMR 7273, F-13397 Marseille, France

Abstract

Seventeen carbazole-fused coumarin-based oxime esters were developed as monocomponent and photocleavable (Type I) initiators of polymerization displaying excellent light absorption properties in the visible range. Compared to the benchmark photoinitiator diphenyl(2,4,6-trimethylbenzoyl)phosphine oxide (TPO), some of them (namely OXE-1 and OXE-5) could furnish photoinitiation performance on par with that of the reference compound upon irradiation with a LED at 405 nm. Photoinitiation mechanism of these photoinitiators is proposed, supported by theoretical calculations, the detection of CO₂ during photopolymerization by mean of Fourier transform infrared spectroscopy (FTIR) and the detection of radical species by electron spin resonance (ESR). Through direct laser write, different objects exhibiting an excellent spatial resolution could be obtained. Parallel to the photoinitiating ability, the different photoinitiators also showed a thermal initiation behavior, meaning that these structures can serve both as thermal- or as photo-initiators on demand. Due to the high sensitivity of these structures to sunlight, OXE-1 and OXE-5 were also investigated as solar photoinitiators (reactive also in Central Europe in winter) and excellent monomer conversions could be obtained within one hour using a multifunctional acrylate monomer (Ebecryl 605). To the best of our knowledge, these two oxime esters

constitute the first examples of sunlight activable oxime esters ever reported in the literature.

Introduction

During the past decades, photopolymerization has been widely used in applications such as coatings, inks, dental materials or 3D/4D printing due to the numerous advantages this polymerization technique offers, including high reaction rates, energy saving and environmentally friendly polymerization conditions, as well as high polymerization efficiency.¹⁻⁵ For photopolymerization, three important parameters have to be considered, namely the photoinitiating system, the monomer and the light source used to activate the photoinitiating system. Upon light irradiation, the photoinitiating system absorbs light and generates radicals. As a result of this, the polymerization process is initiated and the photopolymer can be formed. Therefore, the careful selection of the photoinitiating system plays an important role in the photopolymerization process.

According to the mechanism of free radical photopolymerization, photoinitiating systems can be divided into two distinct categories, namely Type I photoinitiators (i.e. monocomponent systems) and Type II photoinitiators (multicomponent systems requiring a photoinitiator and different co-initiators).⁶⁻⁹ Type I photoinitiators can generate initiating radicals by homolytic cleavage of a selected bond without requiring the presence of additives.¹⁰ Typical commercially available Type I photoinitiators are Irgacure 369, Irgacure 819 and TPO, and these structures have been largely applied in industrial UV curing applications. Considering that Type I photoinitiators are more and more developed by different research groups, numerous oxime esters (OXE) have been reported in the literature, exhibiting an excellent photoreactivity in photopolymerization.¹¹⁻¹³ Photoinitiating ability of OXEs is directly related to the homolytic cleavage of the N-O bond occurring upon photoexcitation. Active free radicals can be generated according to the following steps: (i) generation of iminyl and alkyloxy/aryloxy radicals *via* homolytic cleavage of the N-O bond under light

irradiation, (ii) the generation of carbon centered radicals and release of CO₂ by decarboxylation of the alkyloxy/aryloxy radicals and (iii) the generated radicals can initiate the photopolymerization.¹⁴⁻¹⁷ In addition, release of CO₂ within the photocurable resin is of crucial interest for the polymerization process as it can solve the problem of oxygen inhibition by impeding the diffusion of oxygen within the photocurable resin during photopolymerization. At present, only few OXEs are available for industrial production, such as *O*-benzoyl- α -oxoimine and *O*-acetyloxime, which are both used for pigmented formulations. However, these two OXEs have an obvious limitation since these two molecules can only be efficiently photoexcited around 330 nm. When excited at longer wavelengths i.e. in the near-UV range (385 nm, 395 nm) or with visible light (405 nm, 415 nm, ...) a severe reduction of their photoinitiating abilities is evidenced.¹⁸ Face to these considerations, an urgent need for developing OXEs exhibiting improved light absorption abilities in the near-UV or visible range and exhibiting a high photoreactivity exists at present in photopolymerization.

In our previous works, different OXEs have been developed and reported with different chromophores, such as nitrocarbazoles, triphenylamines, coumarins, pyrenes, anthracenes and naphthalenes.^{10, 14, 19-21} In the literature, many other OXEs exhibiting different chromophores have been reported by different research groups, including chalcones, coumarins, bicarbazoles, phenothiazines, stilbenes, phenyl thienyl thioethers and fluorophenyl.^{13, 16, 22-29} From the reactivity viewpoint, oxime esters based on carbazoles and coumarins both proved to be remarkable Type I photoinitiators, as evidenced in our previous works. In this context, we decided to design a hybrid structure comprising both a carbazole and a coumarin moiety, in which the two groups would be fused, generating a carbazole-fused coumarin structure. It has to be noticed that the carbazole-fused coumarin scaffold has already been used for the design of Type I photoinitiators applied to two-photon polymerization. However, in this previous work, the oxime ester moiety was located on the carbazole side contrarily to what is reported in this work and a laser was used as the light source.^{30, 31}

Parallel to the design of monocomponent photoinitiating systems that contribute to simplify the composition of the photocurable resin, the design of solar photoinitiators

is an active research field as Sun is a renewable and unlimited light source on Earth. However, contrarily to artificial light sources, intensity of sunlight is lower than that of LEDs and the emission spectrum is also broader so that most of the photoinitiators that can be efficiently activated with LEDs can't operate under sunlight.³² To end, polymerization time under sunlight often ranges from a few hours up to more than 10 hours so that the identification of structures that could enable to generate photopolymers with shorter irradiation times are actively researched.

In this work, we successfully synthesized 17 carbazole-fused coumarin-based photoinitiators and their chemical structures are presented in Scheme 1. It has to be noticed that the 17 compounds reported in this work have never previously been reported in the literature, highlighting the novelty of the approach. Only one oxime ester with a structure similar to one of our derivatives i.e. OXE-1 was recently patented. However, the carbazole-fused coumarin scaffold is not unknown in photopolymerization since this structure has been examined in 2022 for the design of photobleachable type II photoinitiators enabling to achieve a deep photocuring under visible light. Interestingly, monocomponent photoinitiating systems were obtained by the concomitant presence of both the ketone and the carbazole moiety enabling to generate α -aminoalkyl radicals. Radical generation could be obtained by mean of an intra and /or intermolecular electron transfer. In our study, the approach is different since a photoreactive group that can homolytically cleave has been introduced on the coumarin side. As specificities, positioning of the photocleavable group on the coumarin side is unprecedented in the design of carbazole-fused coumarin-based oxime esters. Different characterizations were carried out to estimate their photopolymerization behaviors and to determine the photoinitiation mechanism upon visible light irradiation, including UV-visible absorption and fluorescence properties, fluorescence lifetimes, free radical photopolymerization and electron spin resonance spin trapping (ESR-ST) experiments. Direct laser write and thermal polymerization experiments were also carried out with the two formulations exhibiting the highest photoinitiating abilities. Finally, these two best OXEs were also identified as ideal

Commenté [JL1]: All new, even for the synthesis?

Commenté [DF2R1]: yes everything is new

Commenté [DF3]: Preparing method and application of long-wavelength coumarin oxime ester compound
China, CN110330501 A 2019-10-15

Commenté [DF4]: ref à ajouter : Polym. Chem., 2022, 13, 3367 : Fused carbazole-coumarin-ketone dyes: high performance and photobleachable photoinitiators in free radical photopolymerization for deep photocuring under visible LED light irradiation

candidates for photopolymerization experiments done under sunlight. To the best of our knowledge, sunlight activation of oxime esters is unprecedented in the literature.

Experimental Section

Synthesis of OXEs

Synthetic procedures used to access to the different structures OXE-0-OXE-17, are depicted in detail in the supporting information (SI).

Other Materials

The monomers, trimethylolpropane triacrylate (TMPTA) and Ebecryl605 (bisphenol A epoxy diacrylate oligomer diluted with 25% of tripropyleneglycol diacrylate) were both purchased from Allnex (Ivry sur Seine, France) for free radical photopolymerization (RFP). The storage inhibitor was not removed from the monomer prior to the photopolymerization experiments. The commercial photoinitiator, diphenyl (2,4,6-trimethylbenzoyl)phosphine oxide (TPO), was purchased from Sartomer-Lambson (United Kingdom). *N-tert*-butyl- α -phenylnitrone (PBN) was obtained from TCI Europe (Paris, France) and was used as the free radical trapping agent. The colloidal silica suspension (LUDOX AS 30, 30 wt % suspension in H₂O) used to determine the impulse response function of the fluorimeter was obtained from Sigma-Aldrich.

UV-Visible Absorption Properties

UV-Visible absorption spectra of OXEs dissolved in acetonitrile (2×10^{-5} M) were obtained with a JASCO V730 spectrometer (1 cm optical path length). Steady-state photolysis of OXEs dissolved in acetonitrile (2×10^{-5} M) was also performed on a JASCO V730 spectrometer, under irradiation with a 405 nm LED (110 mW.cm^{-2}).

Fluorescence Spectra and Fluorescence Lifetime

Fluorescence spectra of OXEs (concentration in the range of 2×10^{-5} M in methyl alcohol used as the solvent) were investigated on a JASCO FP-750 spectrofluorometer.

Fluorescence excited-state lifetimes were determined with a HORIBA PPD-850 detector.

Singlet excited-state energies (E_{S1} in kcal/mol) of OXEs were calculated from the intersection of the normalized fluorescence emission spectra and the normalized UV-visible absorption spectra and E_{S1} was calculated by equation (1). Enthalpies of the cleavage process of the N-O bond ($\Delta H_{\text{Cleavage}}$) from OXEs were calculated by equation (2) and equation (3), based on the energies of the singlet or triplet excited states (E_{S1} or E_{T1}) and the dissociation energies of the N-O bond (BDE).

$$E_{S1} = 1240/WL \times 23.06 \frac{\text{kcal}}{\text{mol}} \quad \text{equation (1)}$$

$$\Delta H_{\text{Cleavage}_{S1}} = \text{BED}_{(N-O)} - E_{S1} \quad \text{equation (2)}$$

$$\Delta H_{\text{Cleavage}_{T1}} = \text{BED}_{(N-O)} - E_{T1} \quad \text{equation (3)}$$

In equation (1), WL is the x-coordinate of the intersection without unit of the normalized fluorescence emission spectra and the normalized UV-visible absorption spectra.

Free Radical Photopolymerization

First, the different OXEs and the monomer (TMPTA) were mixed in a glass bottle and stirred overnight away from light. The concentration of OXEs in all formulations was controlled to be 2×10^{-5} mol.g⁻¹ in TMPTA, which corresponds to a weight percentage in the range of 0.61 wt% to 0.97 wt% in TMPTA depending on their different molecular masses of OXEs. Concentration of the commercial photoinitiator TPO was controlled at 2×10^{-5} mol.g⁻¹ (0.7 wt%) in TMPTA.

In order to reduce or avoid oxygen inhibition, drops of the homogenous formulations were deposited in a mold to prepare thick sample (1.4 mm) or the laminate between two transparent polypropylene films for thin sample preparation (~25 μm). Subsequently, the kinetics of radical photopolymerization of TMPTA samples when exposed to a 405 nm LED (110 mW.cm⁻²) at room temperature for 600 s was investigated by real-time Fourier transformed infrared (RT-FTIR) spectroscopy (JASCO FTIR-4100). The acrylate characteristic peak area of TMPTA for thin sample

was selected from 1589 to 1665 cm^{-1} and that of TMPTA for thick sample was in the near-infrared range at $\sim 6160 \text{ cm}^{-1}$. The acrylate function conversion (FC) of TMPTA for a given time t was calculated by equation (4):

$$FC(t) = (A_0 - A_t) / A_0 \times 100\% \quad \text{equation (4)}$$

Where A_0 and A_t are the peak area at $t = 0$ s and at any t respectively. The final acrylate conversion was determined by the shape of the conversion curves, which is reached either after a plateau is reached (rate practically zero even under illumination) or after a certain illumination period.

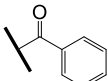
Electron Spin Resonance Spin Trapping (ESR-ST)

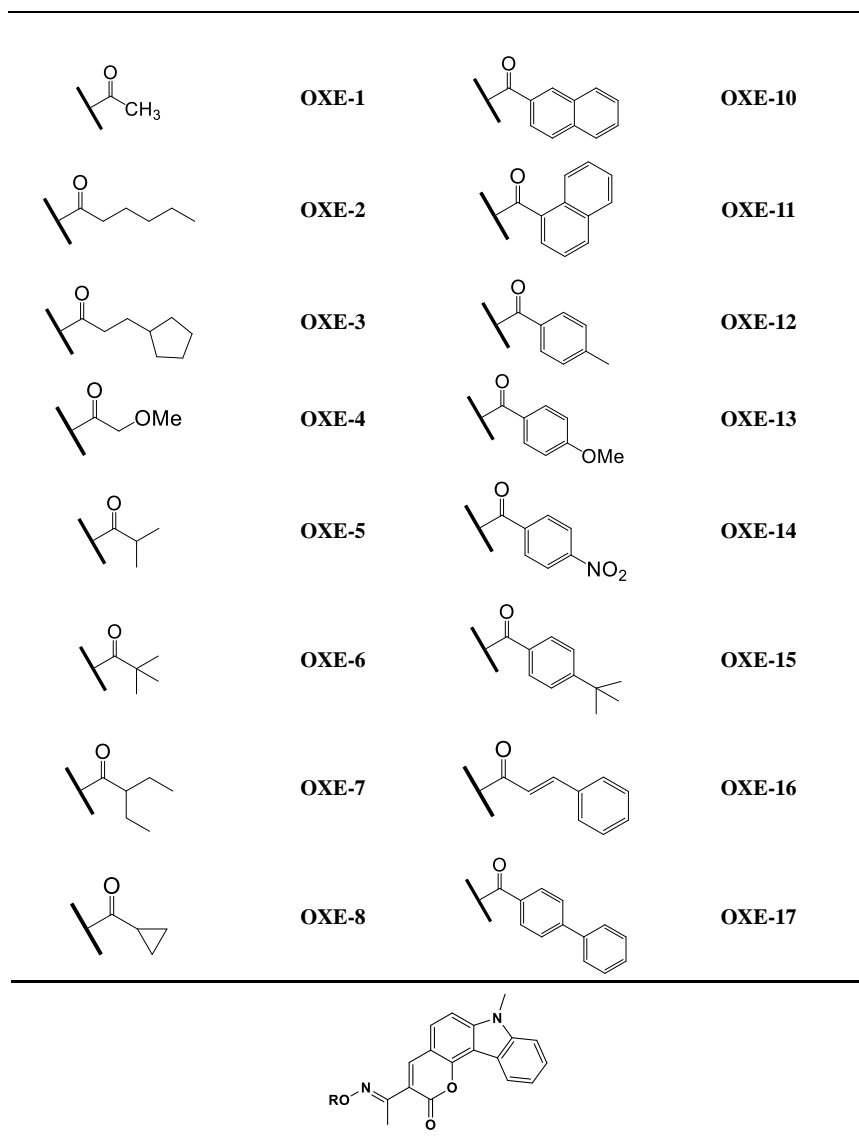
ESR-ST experiments were performed with a X-band spectrometer (Bruker EMX plus). N_2 saturated solution of PBN in *tert*-butylbenzene was selected as the free radical trapping agent, and the concentration of PI dissolved in PBN solution was adjusted to 2×10^{-5} M. During ESR-ST experiments, PBN solvent containing PI was irradiated upon 405 nm LED ($110 \text{ mW} \cdot \text{cm}^{-2}$) at room temperature, inside the cavity of the ESR apparatus. Then, ESR spectrum was recorded after irradiation of 405 nm LED. ESR spectra simulations were performed by WINSIM software.

Direct Laser Write (DLW)

The homogeneous formulation was deposited into a homemade glass tank (2 mm thickness). Then, a laser diode (spot size around 50 μm , 405 nm, and 110 mW) was used as the light source for a spatial irradiation controlled by a computer program to manufacture specific 3D patterns. After DLW process, these 3D patterns were cleaned by acetone to remove the uncured monomer. Finally, a scanning electron microscope (SEM) was used to observe the surface of the printed 3D patterns.

Scheme 1. Chemical Structures of the 17 investigated oxime esters (OXEs) and the corresponding oxime OXE-0.

R	OXE	R	OXE
H	OXE-0		OXE-9



Light Absorption Property

UV-visible absorption spectra of OXEs are shown in Figure 1, and the light absorption properties of all OXEs with different functional groups are listed in Table 1. OXE-14 only showed a poor solubility in acetonitrile. For this reason, no molar extinction coefficient is given for this compound. The other OXEs showed a broad light absorption band tailing up to 450 nm. The maximum absorption wavelength values

(λ_{\max}) of these OXEs are located in the 378-385 nm range (see Table 1). Compared to OXE-0 (with an absorption maximum around 371 nm) that does not comprise an oxime ester group, a red-shift of λ_{\max} for the 17 oxime esters could be detected as shown in Figure 1. This bathochromic shift can be explained by the presence of the oxime ester groups acting as electron-withdrawing groups. As shown in Table 1, compared to ϵ_{\max} of OXE-0 (371 nm, 34500 M⁻¹·cm⁻¹), most of the OXEs had larger ϵ_{\max} values. Furthermore, the $\epsilon_{405\text{nm}}$ values of these OXEs were larger than that of OXE-0, respectively. Therefore, these results indicate that these OXEs can be more sensitive to light irradiation at 405 nm than the parent structure OXE-0.

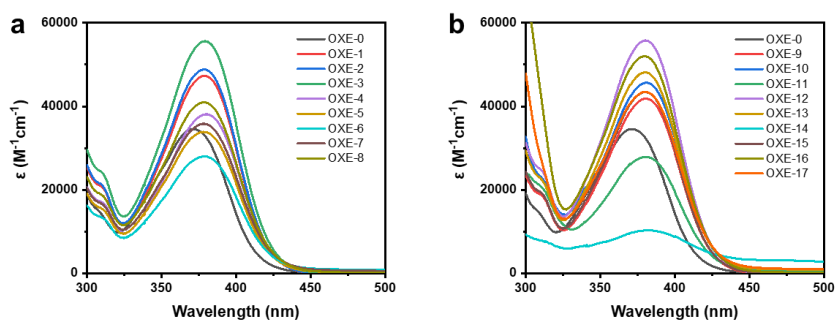


Figure 1. UV-Visible absorption spectra of oxime esters in acetonitrile.

Table 1. Light absorption properties of OXEs in acetonitrile.

OXE	λ_{\max} (nm)	ϵ_{\max} (M ⁻¹ cm ⁻¹)	$\epsilon_{405\text{nm}}$ (M ⁻¹ cm ⁻¹)
OXE-0	371	34500	9800
OXE-1	379	47200	22600
OXE-2	380	48600	23100
OXE-3	378	55500	27300
OXE-4	379	38000	20100
OXE-5	378	33800	16600
OXE-6	379	28000	14300
OXE-7	378	35800	18000
OXE-8	378	40900	20400
OXE-9	380	41800	22600

OXE-10	380	45600	25500
OXE-11	380	27800	15400
OXE-12	380	55700	29700
OXE-13	380	48100	25700
OXE-14	383	-	-
OXE-15	380	43400	23000
OXE-16	380	52000	27500
OXE-17	380	43400	24100

Steady-State Photolysis

As shown in Figures 2, S1 and S2, steady-state photolysis experiments were performed to investigate the photolysis behaviors of the different OXEs upon irradiation. As shown in Figure 2, the absorbance of OXE-0 does not have an obvious decline even after irradiation with a 405 nm LED for 60 s, which means that OXE-0 is unable to initiate the polymerization by a photocleavage reaction. Indeed, OXE-0 is only an oxime and not an oxime ester as the other structures. Conversely, for oxime esters such as OXE-1 and OXE-5, a gradual decline of their absorbances with the irradiation time could be evidenced. This phenomenon is the result of the homolytic cleavage of the N-O bond. Notably, a rapid decline after 10 s of exposure to a 405 nm LED could be detected by UV-visible absorption spectroscopy. Steady-state photolysis spectra of the other OXEs are shown in Figures S1 and S2. Noticeably, a decline of the absorption intensity of OXEs at their maximum absorption wavelengths could be detected upon irradiation at 405 nm.

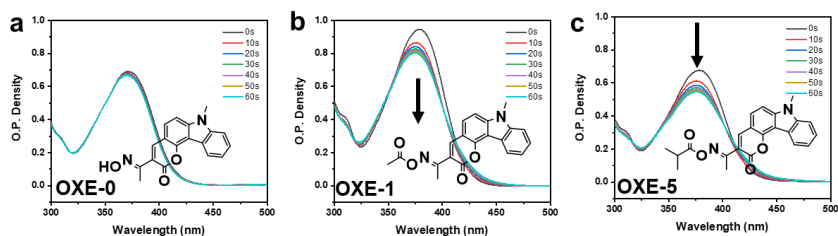


Figure 2. Steady-state photolysis of OXEs in acetonitrile upon irradiation with a 405 nm LED. (a) OXE-0, (b) OXE-1, (c) OXE-5.

The singlet excited-state energies (E_{S1}) of OXEs were obtained from the intersection of their fluorescence emission spectra and their UV-visible absorption spectra (see Figure 3, Figures S3 and S4). The negative $\Delta H_{\text{Cleavage } S1}$ values indicate that the photocleavage of the N-O bond from the singlet excited state is energetically favorable. As listed in Tables 2, all OXEs have favorable $\Delta H_{\text{Cleavage } S1}$ for cleavage. Furthermore, excited state lifetimes of OXEs could be measured (see Figure 3, Figure S5 and Figure S6) and the values are listed in Table 2. Normally, OXEs with a high initiating efficiency have a short excited-state lifetime, which can be beneficial for the cleavage process. In addition, the negative $\Delta H_{\text{Cleavage } S1}$ values also suggest the cleavage process of the N-O bond to be favorable. The cleavage from T_1 is much less favorable energetically (See Table 2).

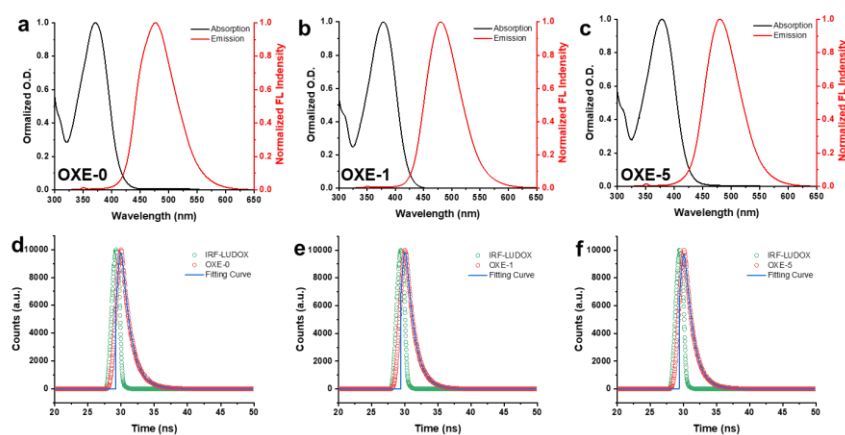


Figure 3. Singlet-state energy determination for (a) OXE-0, (b) OXE-1 and (b) OXE-5, and fluorescence decay curve of (d) OXE-0 (e) OXE-1 and (f) OXE-5.

Table 2. N-O BDE, E_{S1} , E_T , $\Delta H_{\text{Cleavage } S1}$, $\Delta H_{\text{Cleavage } T1}$ and lifetime of different OXEs.

PIs	N-O BDE (kcal.mol ⁻¹)	E_{S1} (kcal.mol ⁻¹)	$\Delta H_{\text{Cleavage } S1}$ (kcal.mol ⁻¹)	E_T (kcal.mol ⁻¹)	$\Delta H_{\text{Cleavage } T1}$ (kcal.mol ⁻¹)	Lifetime (ns)
OXE-0	64.14	68.26	-4.12	45.5	18.64	1.67

OXE-1	47.81	67.20	-19.39	47.97	-0.16	1.52
OXE-2	47.92	67.12	-19.2	47.89	0.03	2.81
OXE-3	47.84	66.85	-19.01	47.87	-0.03	2.09
OXE-4	48.34	66.71	-18.37	48.10	0.24	1.67
OXE-5	47.41	67.10	-19.69	47.98	-0.57	1.56
OXE-6	46.54	67.01	-20.47	47.85	-1.31	2.72
OXE-7	46.85	67.10	-20.25	47.95	-1.1	2.71
OXE-8	47.93	67.17	-19.24	47.87	0.06	1.89
OXE-9	47.29	66.98	-19.69	47.78	-0.49	2.84
OXE-10	47.16	66.43	-19.27	47.74	-0.58	2.75
OXE-11	46.08	66.43	-20.35	47.78	-1.7	2.75
OXE-12	47.03	66.59	-19.56	47.67	-0.64	2.77
OXE-13	46.74	66.56	-19.82	47.51	-0.77	2.81
OXE-14	49.26	68.73	-19.47	48.18	1.08	2.34
OXE-15	47.01	66.51	-19.5	47.65	-0.64	2.67
OXE-16	48.05	66.45	-18.4	47.34	0.71	2.00
OXE-17	47.19	66.54	-19.35	47.70	-0.51	2.39

Free Radical Photopolymerization

Photopolymerization profiles in thin samples are presented in Figure 4 and the final conversions (FCs) and photopolymerization rates (R_p) of the different formulations are listed in Table 3. As shown in Figure 4, compared to the FC of TPO in

TMPTA (63%), OXE-1 (65%), OXE-2 (67%), OXE-5 (68%) and OXE-7 (65%) have the higher FC values, indicating their better photoinitiation performance. Compared to the polymerization rate obtained with the TPO-based formulation ($R_p/[M_0] \times 100 = 7.5 \text{ s}^{-1}$), the larger values of OXE-1 ($R_p/[M_0] \times 100 = 5.6 \text{ s}^{-1}$), OXE-2 ($R_p/[M_0] \times 100 = 6.9 \text{ s}^{-1}$), OXE-5 ($R_p/[M_0] \times 100 = 5.9 \text{ s}^{-1}$) and OXE-7 ($R_p/[M_0] \times 100 = 6.5 \text{ s}^{-1}$) based formulations also indicate their favorable initiation performance. Photopolymerization profiles of thick samples are also presented in Figure S7.

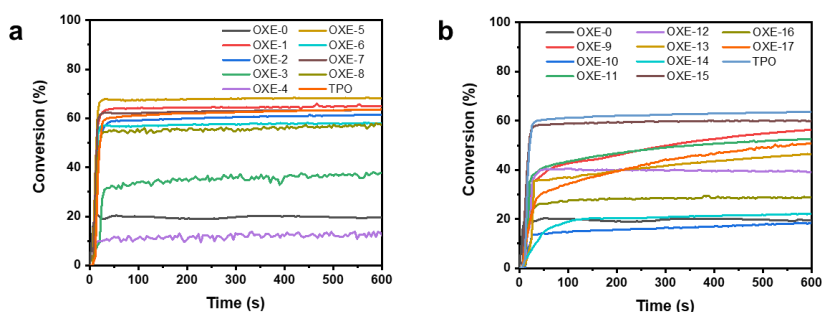


Figure 4. Photopolymerization profiles of TMPTA in laminate ($\sim 25 \mu\text{m}$) upon exposure to a 405 nm LED in the presence of different OXEs ($2 \times 10^{-5} \text{ mol.g}^{-1}$ in TMPTA) and the benchmark photoinitiator TPO. The irradiation starts at $t = 10 \text{ s}$.

Table 3. Final acrylate function conversions (FCs) and photopolymerization rate (R_p) of TMPTA containing different OXEs.

OXE	Final Conversion (FC, %)	$R_p/[M_0] \times 100 \text{ (s}^{-1}\text{)}$
OXE-0	19	0.1
OXE-1	65	5.6
OXE-2	67	6.9
OXE-3	37	3.1
OXE-4	11	1.1
OXE-5	68	5.9
OXE-6	57	5.4
OXE-7	65	6.5
OXE-8	57	5.1
OXE-9	56	1.5

OXE-10	18	1.4
OXE-11	52	3.5
OXE-12	39	8.9
OXE-13	46	4.8
OXE-14	22	0.4
OXE-15	59	3.0
OXE-16	28	1.4
OXE-17	50	1.0
TPO	63	7.5

The Decarboxylation Reaction

For OXEs-based photoinitiating systems, the decarboxylation reaction takes place after a homolytic cleavage of the N-O bond upon irradiation and free radicals can be formed after release of CO₂. Therefore, the decarboxylation reaction was investigated by monitoring the generation of CO₂, which can easily be detected by RT-FTIR (see Figure 5, Figure S8 and Figure S9). As shown in Figure 5.a, the CO₂ absorbance peak (at 2337 cm⁻¹) cannot be clearly observed after 30 s of irradiation during photopolymerization for the oxime OXE-0. The appearance of the CO₂ absorbance peak can be detected for the oxime esters OXE-1 and OXE-5 during photopolymerization, and this phenomenon can also be observed for several other OXE-based systems, such as OXE-2~OXE-4 and OXE-6~OXE-8 (see Figure S7). This clearly proves that a decarboxylation reaction occurred during photopolymerization.

In previous works, our group has reported a series of enthalpy of decarboxylation reaction ($\Delta H_{\text{decarboxylation}}$) and demonstrated that when the $\Delta H_{\text{decarboxylation}}$ was negative, the decarboxylation process was favorable. As previously reported, determination of positive values for $\Delta H_{\text{decarboxylation}}$ of all OXEs bearing aromatic groups on the oxime-ester side is indicative of their inability to decarboxylate. Notably, the $\Delta H_{\text{decarboxylation}}$ values determined for OXE-9, OXE-10 (and OXE-11), and OXE12 are respectively of

5.92, 4.36 (6.24) and 6.92 kcal·mol⁻¹. This could be the explanation why the CO₂ peak cannot be observed during photopolymerization with the three OXE/systems.

As shown in Figure 5.d, the absorbances of CO₂ in OXE-1 and OXE-5 both increase from 10 s to ca. 75 s, related to the generation of CO₂ by the decarboxylation reaction. After t = 60 s, the absorbances of CO₂ start to decrease which may be due to the diffusion from the cured samples to the air. This trend is in agreement with their acrylate function conversions, which increase rapidly accompanied by the generation of CO₂ for the OXE-A1/TMPTA and OXE-B4 systems from 10 s to ca. 75 s. This behavior can be observed for other OXE/TMPTA systems, such as OXE-2~OXE-8 (see Figure S10).

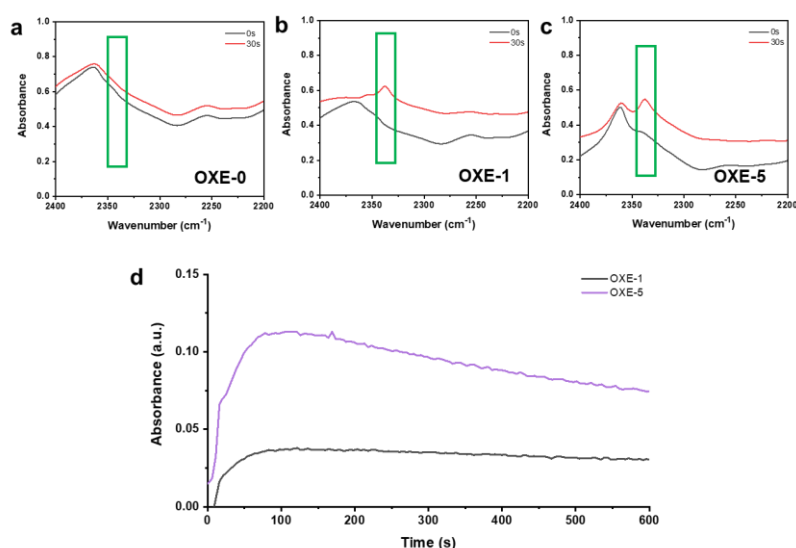


Figure 5. Infrared spectra of (a) OXE-0 in TMPTA, (b) OXE-1 in TMPTA and (c) OXE-5 in TMPTA at t = 10 and 30 s, and (d) the absorption intensity of CO₂ obtained from the OXE-1 or OXE-5/TMPTA systems respectively.

Electron Spin Resonance Spin Trapping (ESR-ST)

After release of CO₂ subsequent to the homolytic cleavage of the N-O bond, carbon-centered radicals can be formed, constituting the reactive and initiating species. Here, ESR-ST experiments were carried on OXE-1 and OXE-5 (see Figure 6 and Figure S14), and alkyl-C(=O)O• radicals were trapped by PBN in each system after 405 nm

Commenté [JL5]: No Figure S14??

irradiation. For OXE-1, the values of the hyperfine coupling constants for alkyl-COO• are $\alpha_N = 13.5$ G and $\alpha_H = 1.8$ G, which can be assigned to the acetyl radical (CH₃COO•). For OXE-5, the values of hyperfine coupling constants are $\alpha_N = 13.7$ G and $\alpha_H = 1.7$ G, which can be assigned to the isobutyryl radical (100%). These ESR results indicate the favorable cleavage process during photopolymerization.

According to the decarboxylation reaction and ESR results, the proposed photoinitiation mechanism is shown in Scheme 2. Upon irradiation at 405 nm with a LED, OXEs can be promoted in the excited state, so that iminyl and acyloxy/aryloxy radicals can be generated from the homolytic cleavage reaction i.e. the dissociation of the N-O bond of OXEs. After this, acyloxy/aryloxy radicals can produce the active free radicals and CO₂ through the decarboxylation reaction.

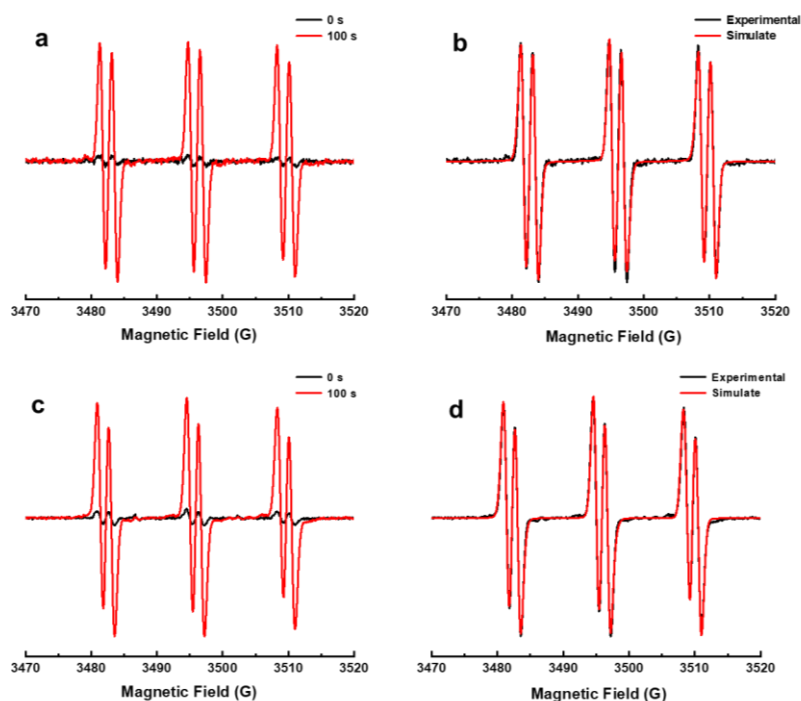
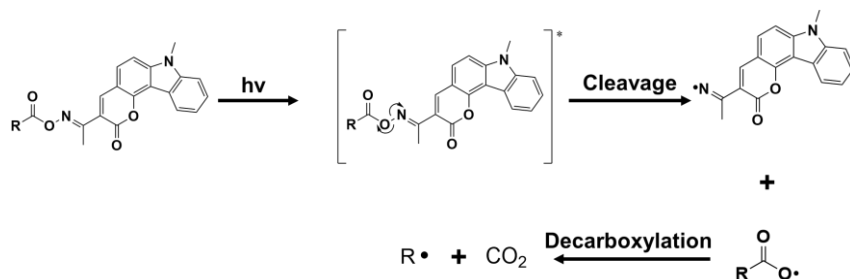


Figure 6. ESR-ST spectra of the PBN radical adducts of (a) and (b) OXE-1, (c) and (d) OXE-5 under LED@405 nm irradiation in *tert*-butylbenzene.



Scheme 2. Proposed photoinitiation mechanism.

Direct Laser Write (DLW) and DSC experiments

OXE-1/TMPTA and OXE-5/TMPTA were used as a model system to carry out DLW, according to their favorable photoinitiation performance. As shown in Figure 7, two thin objects (thickness < 0.33 mm, area < 63 mm², volume < 18.9 mm³) can be successfully obtained within a short time (around 1 min). For OXE-5/TMPTA based object, a good resolution of the object can be clearly observed and the route of laser write also can be clearly detected on the picture. The same phenomenon also can be surveyed on OXE-1/TMPTA based object.

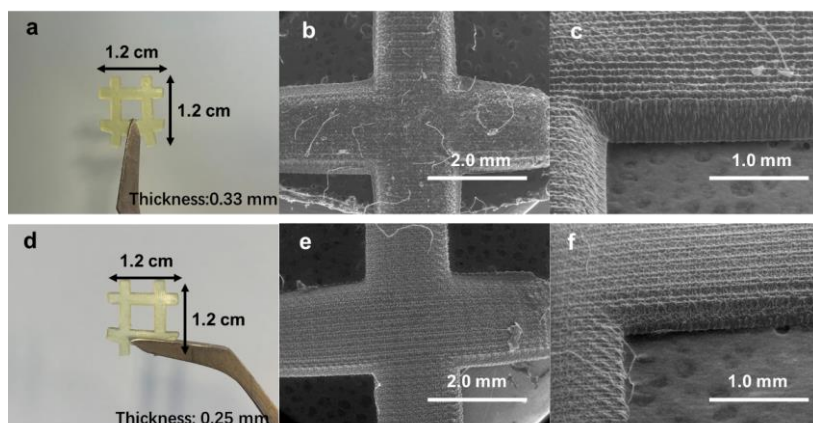


Figure 7. Digital photos of 3D printed objects *via* DLW using (a) OXE-1/TMPTA and (d) OXE-5/TMPTA respectively, and SEM images for (b, c) OXE-1/TMPTA and (e, f) OXE-5/TMPTA.

Thermal Initiation Behavior

Markedly, free radicals in OXEs polymerization systems can also be generated by thermal initiation. DSC thermograms of OXE-0, OXE-1 and OXE-5 in TMPTA are shown in Figure 8 and their parameters (T_{initial} , T_{max} and the final acrylate conversion of TMPTA) are listed in Table 4. T_{initial} values of OXE-0 in TMPTA is 125°C, followed by a weak increase leading to a shoulder at 210°C and a maximum in the 236°C range. This clearly shows that the thermally induced polymerization is slow and superimposed by other thermal effects. For analyzed OXE-1 and OXE-5 have lower T_{initial} values (88.9 and 111.6°C) and lower T_{max} (179.2 and 181.5°C). Interestingly, OXE-1 and OXE-5 showed the dual photo/thermal initiation behavior, which can for example be used for the preparation of carbon fiber composites which are non-transparent and can only be cured thermally or by the dual activation mode namely light plus heat.

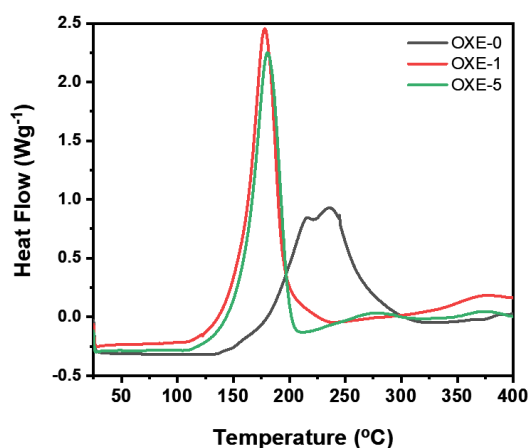


Figure 8. DSC thermograms of OXEs in TMPTA. The presence of oxime esters (OXE-1, OXE-5) clearly moves the thermal initiation to lower temperatures.

Table 4. Parameters about thermal polymerization.

PIs ($2 \times 10^{-5} \text{ mol.g}^{-1}$)	T_{initial} (°C)	T_{max} (°C)	Conversion (%)
OXE-0	128	236	
OXE-1	90	180	60
OXE-5	112	182	54

Sunlight Initiated Polymerization

During the different ESR experiments, we observed that OXE-1 and OXE-5 both have a high sensitivity to daylight. In this context, initiation performance of OXE-1 and OXE-5 in TMPTA and Ebecryl605 respectively under sunlight were investigated on February 10th 2023 in Mulhouse - France (see in SI for the experimental conditions; the weather report is presented in Figure S11). Therefore, 1.4 mm thick samples were prepared in a mold and the IR spectra were measured after the sample had been in direct contact with sunlight (outdoors) for 0, 10, 30 and 60 minutes. From previous studies, we can assume that the reduced total hemispherical radiation $H(t) - D(t)$ and the diffuse sky radiation $D(t)$ on a horizontal surface were in the range of 150 - 350 W/m² and 50 W/m², respectively, for all wavelengths emitted by the solar disk. These conditions were very challenging and nearly 3 times lower than the maximal hemispherical radiation possible under optimal conditions on earth surface. As shown in Figure 9, OXE-1 results in the best initiation performance in Ebecryl605, and the conversion was of 52% after maximal half an hour of exposure to sunlight. A similar phenomenon could be observed with OXE-5/Ebecryl605 (44.5% after 1 hour). However, lower monomer conversions were determined using TMPTA as the monomer. Thus, using OXE-1 and OXE-5 as photoinitiators, conversions of 15.4 and 9.2% were respectively determined. We assume that differences in the viscosity / oxygen solubility / oxygen inhibition are more (more inhibition with TMPTA than Ebecryl 605). Despite the low TMPTA conversions obtained with these two OXEs, these results clearly indicate that OXE-1 and OXE-5 can promote sunlight driven polymerization processes and can be facily excited with sunlight. This result is unprecedented in the literature for oxime esters.³³ To the best of our knowledge, no oxime esters activable with sunlight has been reported yet.

Commenté [MS6]: At the inside behind a window or at the outside ???!

Film, thickness, expermenet is not clear. Please check if my suggestion is correct

Commenté [MS7]: Add references

Schmitt, M.; Heib, F., About the possibility of calibrating optical detectors by solar radiation. *RSC Advances* **2014**, *4*, 17639-17647.

Schmitt, M., Synthesis and testing of ZnO nanoparticles for photo-initiation: Experimental observation of two different non-migration initiators for bulk polymerization. *Nanoscale* **2015**, *7*, 9532-9544.

Commenté [MS8]: 15 – 35 W/cm² and 5 W/cm² ?! (*1000/10000)

Commenté [MS9]: Schmitt, M.; Heib, F., About the possibility of calibrating optical detectors by solar radiation. *RSC Advances* **2014**, *4*, 17639-17647.

Commenté [MS10]: Accuracy is to exact

52
45
15
9

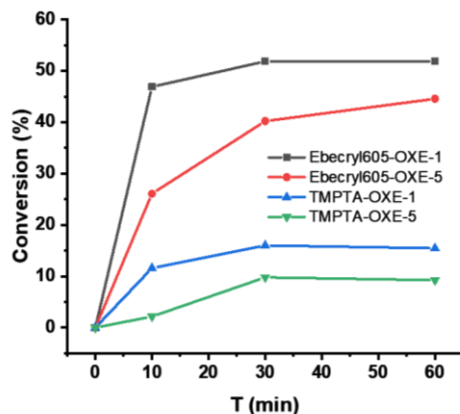


Figure 9. Sunlight initiating photopolymerization for OXE-1 and OXE-5 based system respectively (thick samples, 1.4 mm).

CONCLUSION

In this work, we successfully designed and synthesized 17 new carbazole-fused coumarins-based oxime esters (OXEs) and none of these structures have been previously reported in the literature. Especially, introduction of the photocleavable group on the coumarin side is innovative for carbazole-fused coumarins. Among these OXEs, OXE-1 and OXE-5 exhibited good light absorption properties and good photolysis performance upon LED@405nm irradiation at room temperature. These two OXEs showed better performance than the commercial photoinitiator TPO. OXE-1 or OXE-5-based formulations could be used to elaborate 3D objects *via* direct laser write. Interestingly, OXE-1 and OXE-5 both could also be employed as thermal initiators for the FRP of TMPTA. Among the most interesting results of this study, OXE-1 or OXE-5 could efficiently promote the polymerization of Ebecryl605 under sunlight irradiation (Central Europe in Winter), what is unprecedented in the literature. Indeed, no sunlight sensitive oxime esters has been reported in the literature yet. Through RT-FTIR spectra and ESR-ST results, the mechanism of photocleavage and occurrence of a decarboxylation reaction could be clearly demonstrated. Therefore, this work opens new perspectives for the design of sunlight activable oxime-esters and future works will consist in improving the photoreactivity of oxime esters under sunlight. Indeed, at

Commenté [JL11]: How many are completely new?

Commenté [MS12]: Formulations based on OXE-1 or OXE-5 can be used for the production of 3D objects by direct laser writing (405 nm).

present, an irradiation time of around 30 min. is required to get a full curing of the resins, what will certainly be reduced in the future by optimizing the structure of the chromophore.

ASSOCIATED CONTENT

Supporting Information. Steady-state photolysis of OXE-2~OXE-4 and OXE-6~OXE-8 in acetonitrile upon the irradiation of 405 nm LED (Figure S1), Steady-state photolysis of OXE-9~OXE-17 in acetonitrile upon the irradiation of 405 nm LED (Figure S2), Singlet-state energy determination of OXE-2~OXE-4 and OXE-6~OXE-8 (Figure S3), Singlet-state energy determination of OXE-9~OXE-17 (Figure S4), Fluorescence decay curve of OXE-2~OXE-4 and OXE-6~OXE-8 (Figure S5), Fluorescence decay curve of OXE-9~OXE-17 (Figure S6), Photopolymerization profiles of TMPTA in laminate (1.4 mm) upon exposure to 405 nm LED in the presence of different OXEs (2×10^{-5} mol.g⁻¹ in TMPTA) (Figure S7), Infrared spectra of TMPTA containing OXE-2~OXE-4 and OXE-6~OXE-8 respectively at t = 10 and 30 s (Figure S8), Infrared spectra of TMPTA containing OXE-9~OXE-17 respectively at t = 10 and 30 s (Figure S9), The absorption intensity of CO₂ obtained from the TMPTA based system containing OXE-2~OXE-4 and OXE-6~OXE-8 respectively (Figure S10), The weather report of February 10th 2023 in Mulhouse, France (Figure S11), and General and detailed information of OXEs Syntheses.

AUTHOR INFORMATION

Corresponding Author

Jacques Lalevée, Université de Haute-Alsace, CNRS, IS2M UMR 7361, F-68100 Mulhouse, France; Université de Strasbourg, France; E-mail : jacques.lalevee@uha.fr

Frédéric Dumur, Aix Marseille Univ, CNRS, ICR, UMR 7273, F-13397 Marseille, France; E-mail : frederic.dumur@univ-amu.fr

Funding

The authors thank the Agence Nationale de la Recherche for fundings provided by the ANR PhotoFlat. Zheng Liu acknowledges the financial support from the Chinese Scholarship Council (CSC) for his Ph.D. studies.

Author Contributions

The manuscript was written through contributions of all authors. All authors have given approval to the final version of the manuscript. The two first authors i.e. Yijun Zhang and Zheng Liu equally contributed to this work.

Notes

The authors declare no competing financial interest. The raw/processed data required to reproduce these findings can be furnished on demand.

ABBREVIATIONS

OXE, oxime ester; TPO, diphenyl(2,4,6-trimethylbenzoyl)phosphine oxide; LEDs, light-emitting diodes; ESR-ST, electron spin resonance spin trapping; TMPTA, trimethylolpropane triacrylate; FRP, free radical photopolymerization; PBN, *N-tert-Butyl- α -phenylnitrene*; IRF, impulse response function; E_{S1} , singlet excited-state energies; E_{T1} , triplet excited states; S_1 , singlet excited states; T_1 , triplet excited states; $\Delta H_{\text{Cleavage}}$, enthalpies of the cleavage process of the N-O bond; BDE, the dissociation energies of the N-O bond; WL, x-coordinate of the intersection of the intersection of the normalized fluorescence emission spectra and the normalized UV-vis absorption spectra; RT-FTIR, real-time Fourier transformed infrared; FC, final conversion; λ_{max} , the maximum wavelength of absorption; ϵ_{max} , the molar extinction coefficients at maximum absorption wavelength; $\epsilon_{405\text{nm}}$, the molar extinction coefficients at 405 nm; DLW, direct laser write; $\Delta H_{\text{decarboxylation}}$, enthalpy of decarboxylation reaction; photopolymerization rate (R_p).

Reference

1. F. Zhang, L. Zhu, Z. Li, S. Wang, J. Shi, W. Tang, N. Li and J. Yang, *Addit. Manuf.*, 2021, **48**, 102423-102442.
2. M. A. Tasdelen, J. Lalevée and Y. Yagci, *Polym. Chem.*, 2020, **11**, 1111-1121.

-
3. H. Mokbel, B. Graff, F. Dumur and J. Lalevee, *Macromol. Rapid Comm.*, 2020, **41**, 2000289-2000293.
 4. X. Zhao, Y. Zhao, M.-D. Li, Z. a. Li, H. Peng, T. Xie and X. Xie, *Nat. Commun.*, 2021, **12**, 2873-2880.
 5. Y. Zhang, Y. Xu, A. Simon-Masseron and J. Lalevee, *Chem. Soc. Rev.*, 2021, **50**, 3824-3841.
 6. X. Ma, D. Cao, H. Fu, J. You, R. Gu, B. Fan, J. Nie and T. Wang, *Prog. Org. Coat.*, 2019, **135**, 517-524.
 7. F. Hammoud, A. Hijazi, S. Duval, J. Lalevée and F. Dumur, *Eur. Polym. J.*, 2022, **162**, 110880-110891.
 8. S. Liu, D. Brunel, G. Noirbent, A. Mau, H. Chen, F. Morlet-Savary, D. Gimes, P. Xiao, F. Dumur and J. Lalevée, *Mater. Chem. Front.*, 2021, **5**, 1982-1994.
 9. K. Sun, Y. Xu, F. Dumur, F. Morlet-Savary, H. Chen, C. Dietlin, B. Graff, J. Lalevée and P. Xiao, *Polym. Chem.*, 2020, **11**, 2230-2242.
 10. Z.-H. Lee, F. Hammoud, A. Hijazi, B. Graff, J. Lalevée and Y.-C. Chen, *Polym. Chem.*, 2021, **12**, 1286-1297.
 11. Y. Pang, S. Fan, Q. Wang, D. Oprych, A. Feilen, K. Reiner, D. Keil, Y. L. Slominsky, S. Popov, Y. Zou and B. Strehmel, *Angew. Chem. Int. Ed. Engl.*, 2020, **59**, 11440-11447.
 12. W. Qiu, M. Li, Y. Yang, Z. Li and K. Dietliker, *Polym. Chem.*, 2020, **11**, 1356-1363.
 13. X. Wu, S. Gong, Z. Chen, J. Hou, Q. Liao, Y. Xiong, Z. Li and H. Tang, *Dyes Pigm.*, 2022, **205**, 110556-111565.
 14. F. Dumur, *Eur. Polym. J.*, 2022, **175**, 111330-111360.
 15. W. Yin and X. Wang, *New J. Chem.*, 2019, **43**, 3254-3264.
 16. Y. Zhang, F. Morlet-Savary, M. Schmitt, B. Graff, A. Rico, M. Ibrahim-Ouali, F. Dumur and J. Lalevée, *Dyes Pigm.*, 2023, **215**, 111202-111214.
 17. F. Hammoud, A. Hijazi, M. Schmitt, F. Dumur and J. Lalevée, *Eur. Polym. J.*, 2023, **188**, 111901-111932.
 18. D. E. Fast, A. Lauer, J. P. Menzel, A.-M. Kelterer, G. Gescheidt and C. Barner-Kowollik, *Macromolecules*, 2017, **50**, 1815-1823.

-
19. S. Liu, N. Giacoletto, M. Schmitt, M. Nechab, B. Graff, F. Morlet-Savary, P. Xiao, F. Dumur and J. Lalevée, *Macromolecules*, 2022, **55**, 2475-2485.
 20. F. Hammoud, N. Giacoletto, G. Noirbent, B. Graff, A. Hijazi, M. Nechab, D. Gigmes, F. Dumur and J. Lalevée, *Mater. Chem. Front.*, 2021, **5**, 8361-8370.
 21. Z. H. Lee, S. C. Yen, F. Hammoud, A. Hijazi, B. Graff, J. Lalevee and Y. C. Chen, *Polymers*, 2022, **14**, 5261-5273.
 22. Z. Li, X. Zou, G. Zhu, X. Liu and R. Liu, *ACS Appl. Mater. Inter.*, 2018, **10**, 16113-16123.
 23. R. Zhou, H. Pan, D. Wan, J.-P. Malval and M. Jin, *Prog. Org. Coat.*, 2021, **157**, 106306-106314.
 24. Y. Ding, S. Jiang, Y. Gao, J. Nie, H. Du and F. Sun, *Macromolecules*, 2020, **53**, 5701-5710.
 25. W. J. Lee, H. S. Kwak, D.-r. Lee, C. Oh, E. K. Yum, Y. An, M. D. Halls and C.-W. Lee, *Chem. Mater.*, 2021, **34**, 116-127.
 26. S. Chen, M. Jin, J.-P. Malval, J. Fu, F. Morlet-Savary, H. Pan and D. Wan, *Polym. Chem.*, 2019, **10**, 6609-6621.
 27. W. Wang, M. Jin, H. Pan and D. Wan, *Dyes Pigm.*, 2021, **192**, 109435-109445.
 28. W. Wang, M. Jin, H. Pan and D. Wan, *Prog. Org. Coat.*, 2021, **151**, 106019-106030.
 29. A. Noon, F. Hammoud, B. Graff, T. Hamieh, J. Toufaily, F. Morlet-Savary, M. Schmitt, T. T. Bui, A. Rico, F. Goubard, S. Péralta, F. Dumur and J. Lalevée, *Adv. Mater. Technol.*, 2023, DOI: 10.1002/admt.202300205, 2300205-2300218.
 30. Z. Liu and F. Dumur, *Eur. Polym. J.*, 2022, **177**, 111449.
 31. R. Zhou, X. Sun, R. Mhanna, J.-P. Malval, M. Jin, H. Pan, D. Wan, F. Morlet-Savary, H. Chaumeil and C. Joyeux, *ACS Appl. Polym. Mater.*, 2020, **2**, 2077-2085.
 32. J. Lalevée and J. P. Fouassier, *Polym. Chem.*, 2011, **2**, 1107-1113.
 33. F. Dumur, *Eur. Polym. J.*, 2023, **189**.

TOC

